Article

Machine Learning Approaches for Designing Meso-scale Structure of Li-ion battery Electrode

Yoichi Takagishi [1]*, Takumi Yamanaka [1] and Tatsuya Yamaue [1]

[1] Kobelco Research Institute Inc., Kobe 6512271, Japan; takagishi.yoichi@kki.kobelco.com; yamanaka.takumi@kki.kobelco.com; yamaue.tatsuya@kki.kobelco.com

* Correspondence: takagishi.yoichi@kki.kobelco.com; Tel.: +81-78-992-5976

Abstract: We have proposed a data-driven approach for designing mesoscale porous structures of Li-ion battery electrode with three-dimensional virtual structures and machine learning techniques. Over 2,000 artificial 3D structures assuming positive electrode composed of random packed spheres as active material particles are generated, and charge/discharge resistance has been evaluated using simplified Physico-chemical model. In this model, resistance from Li diffusion in active material particles (diffusion resistance), transfer resistance of Li+ in electrolyte (electrolyte resistance) and reaction resistance on the interface between active material and electrolyte are simulated based on mass balance of Li, Ohm's law in and linearized Butler-Volmer equation, respectively. Using these simulation results, regression models via Artificial Neural Network (ANN) have been created in order to predict charge/discharge resistance from porous structure features. In this study, porosity, active material particle size and volume fraction, pressure in the compaction process, electrolyte conductivity, and binder/additives volume fraction are adopted as features, associated with controllable process parameters for manufacturing battery electrode. As results, the predicted electrode resistance by ANN regression model is good agreement with the simulated values. Furthermore, sensitivity analysis and optimization of the process parameters have been carried out. The proposed data-driven approach could be a solution as a guiding principle for manufacturing battery electrode.

Keywords: Li-ion battery, electrode, porous structure, virtual structure, machine learning, simulation, physico-chemical model, optimization

1. Introduction

Li-ion secondary batteries have been receiving increasing attention because they have been used in various products including Laptop PC and Electric Vehicles [1]. In spite of their remarkable advancements for the past decades, a higher energy and power density, safer electrodes and electrolytes, and longer durability are still required [2]. In order to satisfy these demands, designing of battery electrodes plays a key role in addition to developing new materials for the electrodes and electrolytes [3,4].

Numerical simulation techniques are powerful tool for prediction of the battery performance from the process parameters of the electrodes. The one-dimensional Physico-chemical simulation models have been used widely in order to predict not only the battery performance [5-6], but also durability [7-9] and safety [10,11]. Although the calculation load is lower in these models, the meso-scale porous structures of the electrodes are not reflected because these structures are approximated as homogeneous solid and liquid state. On the other hand, the three-dimensional extended simulations using 3D-SEM tomography data [12,13] or artificial structure [14,15] based on the Physico-chemical model have been developed and reported recently. Since the meso-scale structures of the porous electrodes are taken into account and three-dimensional distribution of the

electrochemical reaction and Li/Li concentration are estimated in these detailed model, more accurate prediction of battery performance are expected.

Recently, parametric studies and sensitivity analyses of the process parameters using Artificial Neural Networks (ANNs) combined with the Physico-chemical models have been carried out [16, 17]. In these papers, it has been proved that ANNs are useful tool for regression of the battery performance and analysis of the importance features. However, in most cases the one-dimensional homogeneous model has been used because these studies need a large amount of simulation cases. Therefore, it is still unclear the sensitivity and the optimized three-dimensional meso-scale structure of the electrode and process parameters for the battery performance.

In this study, we propose the prediction and optimization scheme of three-dimensional porous electrode of Li-ion battery using high-throughput simulation model and machine learning techniques. First, the high-throughput Physico-chemical modeling based on particles aggregated structures assuming positive electrode are developed and the database of the relationship between the process parameters and the battery performance are construct. Next, development of the regression model of the battery resistance and capacity are created using controllable condition parameters (Active material volume fraction, size etc.) via ANN. Finally, the optimized electrode structures and the process parameters are searched by Bayesian optimization.

2. Simulation Method

2.1. Simulation scheme

Figure 1 illustrates the proposed prediction and optimization scheme of Li-ion battery porous electrode. In the first step, high-throughput Physico-chemical modeling based on particles aggregated structures are developed and the database of the relationship between the process parameters including particle volume fraction, particle radius etc. and the battery performance represented by charge/discharge resistance and capacity are construct. In the second step, the regression model in order to predict the charge/discharge resistance is developed using process parameters as predictors via Artificial Neural Network (ANN). The optimized electrode structures and the process parameters are searched by Bayesian optimization in the final step.

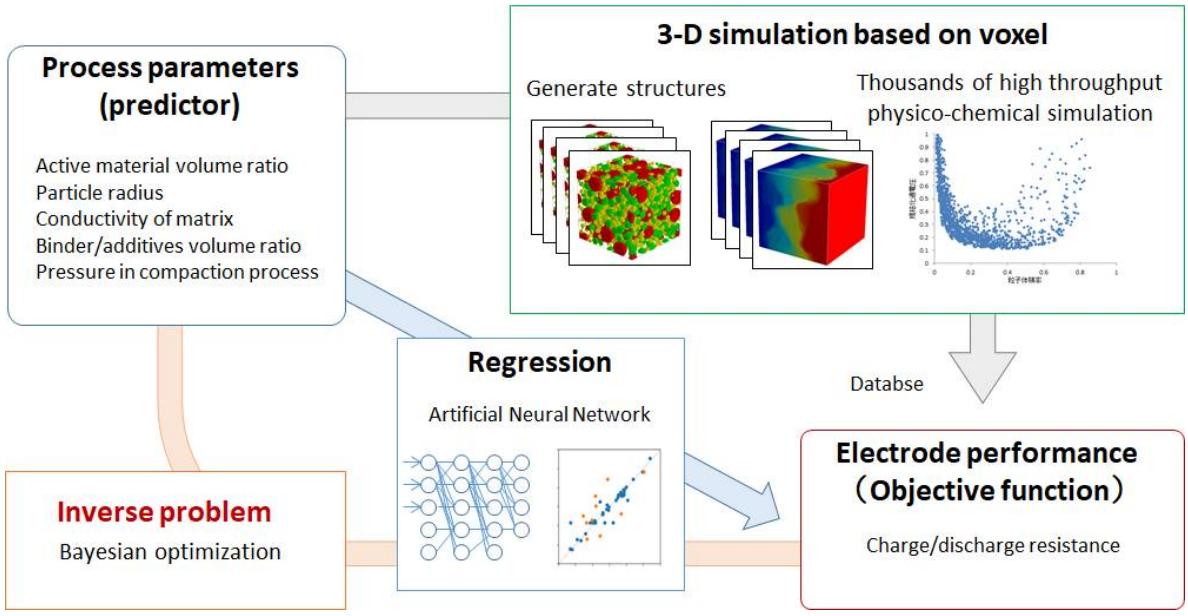

Figure 1. Proposed prediction and optimization scheme of Li-ion battery porous electrode.

2.2. Generation of three-dimensional virtual structure of active material

Preprints (www.preprints.org) | NOT PEER-REVIEWED | Posted: 1 April 2019 doi:10.20944/preprints201904.0016.v1

Peer-reviewed version available at Batteries 2019, 5, 54; doi:10.3390/batteries5030054

Total 2,100 three-dimensional artificial electrode structures composed of hundreds of aggregated particles are generated for evaluation of battery electrode resistance. Fig.2 (a) shows the flow chart to generate artificial structures with parameters based on random packed method [18] using MATLAB code. The active material particle radius (2.5 – 12.5 [um]) is extracted randomly with uniform distribution, and spheres are generated in a 50 x 50 x 50 [um^3] box until the volume fraction reaches the randomly specified value. Compaction process of electrode (calendaring) affects meso-scale structure of pore region and active material particles. Here, maximum overlap length δ between active material particles is estimated from compaction pressure P and the number of active material particle using theoretical model [19],

$$a = \left(3Fr/4E\right)^{\frac{1}{3}} \tag{1}$$

$$\delta = r - \sqrt{r^2 - a^2} \tag{2}$$

where a, r and E means the radius of contact area, the radius of the particle and Yong's modulus (assuming 1.0 [GPa]), respectively. The force between the particles F is estimated as $PS/N_{ap}^{\frac{1}{3}}$ where S and N_{ap} indicates the cross section area of the system and the number of particles, respectively. The generated meso-porous structures of the electrode are shown in Fig.2 (b).

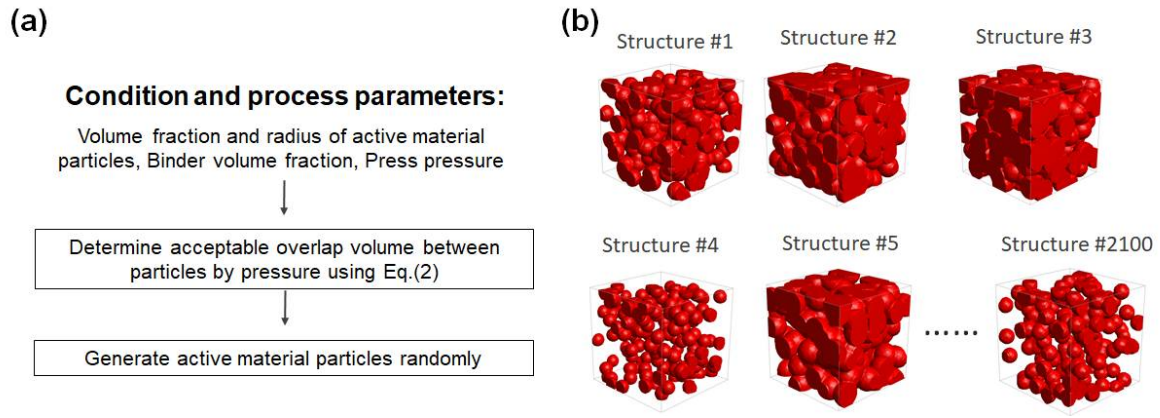

Figure 2. (a) The flow chart to generate the artificial structure with controllable process parameters. (b) The generated meso-porous structures of the electrode.

2.3. Estimation of surface area of pore region and volume fraction of active material

In manufacturing process of electrode, binder and conductive aid are added in active material particles in order to improve its adhesion and conductivity. Although the prediction technique of 3D binder structure in porous materials has been proposed [20], it is still difficult to reproduce the accurate structure of them. In this study, binder and additive region are not modeled explicitly in 3D structure but assumed to be completely mixed and homogeneous in order to estimate the effective porosity and surface area of active material. The volume fraction of homogeneous binder/additives region θ_b is estimated by the volume fraction of pore region θ_p and N_{ap}. The effective volume fraction of pore region $\theta_{p,eff}$ and the effective surface area $S_{p,eff}$ are estimated as

$$\theta_{p,eff} = \theta_p - \theta_b = \theta_p\left(1 - \alpha N_{ap}\right) \tag{4}$$

$$S_{p,eff} = S_p\theta_{p,eff}/\theta_{p,eff} \tag{5}$$

2.4. Simplified Physico-chemical model

Using generated structures described in Section 2.2, the simplified Physico-chemical model has been applied in order to evaluate the resistance and capacity in each structure. The effective conductivity of electrolyte is evaluated Poisson equation in 3D structure,

$$\nabla \cdot \left[-\sigma_l \nabla \phi_l \right] = 0 \tag{6}$$

where σ_l and ϕ_l means the bulk electrolyte conductivity and potential, respectively. The electrolyte resistance R_l is estimated from the effective conductivity of electrolyte $\sigma_{l,eff}$,

$$R_l = \left[\sigma_{l,eff} \left(1-\theta_b\right)^{1.5} \right]^{-1} \tag{7}$$

The calculation has been performed using GeoDict (Math2Market GmbH) [21].

The reaction resistance R_{reac} between the active material and the electrolyte is evaluated by linearized Butler-Volmer equation:

$$i = i_0 \left[\exp\left(\frac{\alpha F}{RT}\eta\right) - \exp\left(-\frac{\alpha F}{RT}\eta\right) \right] \cong i_0 \frac{2\alpha F}{RT}\eta \tag{8}$$

$$R_{reac} = \eta / \left(I \cdot L\right) \tag{9}$$

where i_0, i, η, α, F, R *and* T denotes the exchange current density, current density per surface area of active material overpotential, transfer coefficient, Faraday constant, Gas constant and temperature, respectively. I and L means current density per cross section and system length, respectively.

Li diffusion in the active material is described as steady state diffusion equation using diffusion coefficient D_s,

$$\nabla \cdot \left[-D_s \nabla c_s \right] = 0 \tag{10}$$

where c_s indicates Li concentration in the active material. In this study, Eq. (9) is simplified assuming single sphere particle

$$\Delta c_s = i_s \, r^2 / 2D_s \tag{11}$$

where Δc_s means concentration polarization. Therefore, Li diffusion resistance can be estimated as

$$R_{diff} = \left[\phi_{ocv}\left(c_0\right) - \phi_{ocv}\left(c_0 + \Delta c_s\right) \right] / \left(I \cdot L\right) \tag{12}$$

using average Li concentration in active material c_0 and Open Circuit Voltage (OCV) function

$$\phi_{ocv}\left(c_0\right) = \sum_i p_i \left(c_0 / c_{\max}\right)^i \tag{13}$$

where c_{max} means coefficient and maximum Li concentration of active material. p_i indicates coefficient of polynomial OCV function showed in Table 1. These simplifications make it possible to reduce the calculation load in three-dimensional complex structures.

Table 1. Coefficients of polynomial OCV function [9].

Coefficient	Value
p_6	-43.8299
p_5	109.273
p_4	- 99.9523
p_3	39.8270
p_2	- 5.52739
p_1	- 1.00539
p_0	4.19987

Preprints (www.preprints.org) | NOT PEER-REVIEWED | Posted: 1 April 2019 doi:10.20944/preprints201904.0016.v1

Peer-reviewed version available at Batteries 2019, 5, 54; doi:10.3390/batteries5030054

In order to evaluate charge/discharge resistance and capacity, typical electrochemical parameters are employed of so called NCM, lithium nickel manganese cobalt oxide, positive electrode which is one of oxide material, as shown in Table 1.

Table 1. The parameters for the simplified Physico-chemical model.

Parameter	Value
Exchange current density, i_0	0.10 [A/m^2] *
Temperature, T	298 [K]
Transfer coefficient, α	0.50*
Diffusion coefficient in active material, D_s	5.0×10^{-13} [m^2/s] *
Current density, i	20 [A/m^2]
Maximum Li concentration of active material, c_{max}	26400 [mol/m^3]*

* Assumed value

2.5. Machine learning model

Based on the simulation results described in Section 2.3, ANN models are created as a regression model of the battery resistance using the controllable condition parameters (Active material volume fraction, size etc.). Table 2 shows the dataset for learning and testing including predictors and descriptors. 70% of the data has been taken at random for training, and remaining data has been used for validation of the ANN using R^2 value.

Table 2. The dataset for learning and testing including the predictors and descriptors.

#	Descriptors					Predictors		
	Active material		Binder/ additives	Electrolyte	Compaction process	Reaction resistance	Electrolyte resistance	Diffusion resistance
	Volume fraction	Radius	Volume ratio	Conductivity	Pressure			
	[%]	[um]	[%]	[S/m]	[MPa]	[Ω・m]	[Ω・m]	[Ω・m]
1	77.8	10.5	28.5	0.77	3.12	1.03	291	9.68
2	85.4	11.5	0.254	0.35	23.2	1.71	20.4	4.02
…	…	…	…	…		…	…	
2100	85.4	11.5	0.852	0.35	14.6	1.75	80.7	2.49

Although there is a lot of machine learning models such as LASSO [22] and Ridge regression [23] based on linear regression techniques, ANN based on nonlinear regression is one of the useful tools in order to predict complex relationships between inputs and outputs or to find some patterns in datasets [24]. In this study, the ANN model are constructed with three hidden layers between the input and the output and 20 neurons with sigmoid transfer function. The 70% of the dataset are sampled randomly for training, and remaining 30% are used for testing.

Furthermore, inverse analysis of the process parameters from the total resistance has been carried out using ANN and Bayesian optimization. In this model, the process parameters are initialized randomly and implemented the next candidate with Maximum Likelihood Estimation (MLE). Expected improvement method is adopted as acquisition function with Matern 5/2 kernel function.

ANN modeling and Bayesian optimization have been performed using Scikit-learn [25] and GPyopt [26] of Python Machine Learning library.

3. Results and Discussion

3.1. Sensitivity Analysis of each resistance

The sensitivity analysis of the charge/discharge resistance to the process parameters has been carried out. Fig.3 shows the sensitivities of the reaction resistance, the electrolyte resistance and the Li diffusion resistance to the volume ratio of the active material with total 2,100 simulation results. As the volume ratio increases the reaction resistance decreases dramatically because the effective surface area and the capacity itself increase. On the other hand, the electrolyte resistance increases with the volume ratio exponentially since the electrolyte conductive region, which is pore region, decreases with volume fraction of the active material. The Li diffusion resistance is relatively low in all condition of this study without vicinity of volume fraction 0. Therefore, the total resistance, which is sum of these four resistances, has minimum value to the volume ratio of the active material particles. Thus, there exists the optimum value of the volume ratio of the active material.

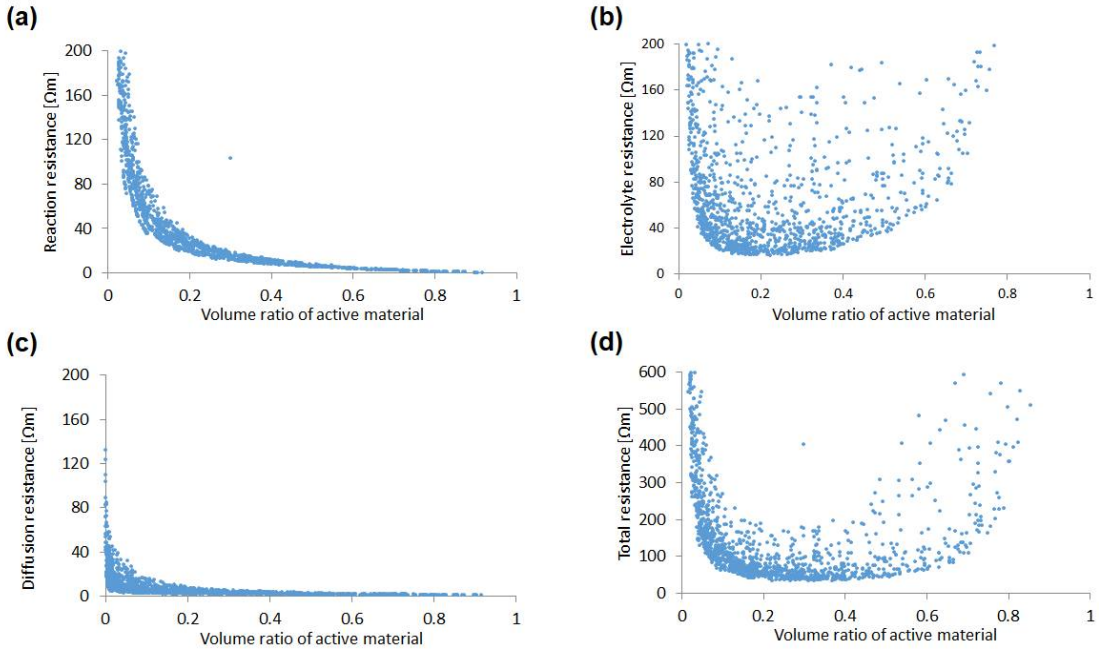

Figure 3. Sensitivities of (a) reaction resistance, (b) electrolyte resistance, (c) Li diffusion resistance, and (d) total resistance to the volume ratio of the active material with total 2,100 simulation results.

In the same manner, the sensitivity analysis has been performed to the active material particle size. As shown in Fig.4, the reaction resistance decreases gradually as the particle size increases. This result is unexpected since the larger particle has smaller surface area and the reaction resistance is supposed to increase as the particle size increases. The reason of this is that the systems composed of smaller particles have larger amount of particles and binder/additives to connect between particles, therefore the effective surface area of the active material particles of the system decreases. Similarly, the electrolyte resistance has higher value in the region under 4 [um] of the particle size. In this region, the effective electrolyte conductivity decreases since the pore space is occupied by binder/additives according to Eq. (2). As a result, the smaller particles are not always effective to decrease the reaction resistance in this study. On the other hands, the diffusion resistance is relatively small to other resistances in each particle size. Therefore, the total resistance has also minimum value to the active material particle size. In other words, there exists optimum value of the particle size as well as the volume ratio of the active material.

Preprints (www.preprints.org) | NOT PEER-REVIEWED | Posted: 1 April 2019 doi:10.20944/preprints201904.0016.v1

Peer-reviewed version available at Batteries 2019, 5, 54; doi:10.3390/batteries5030054

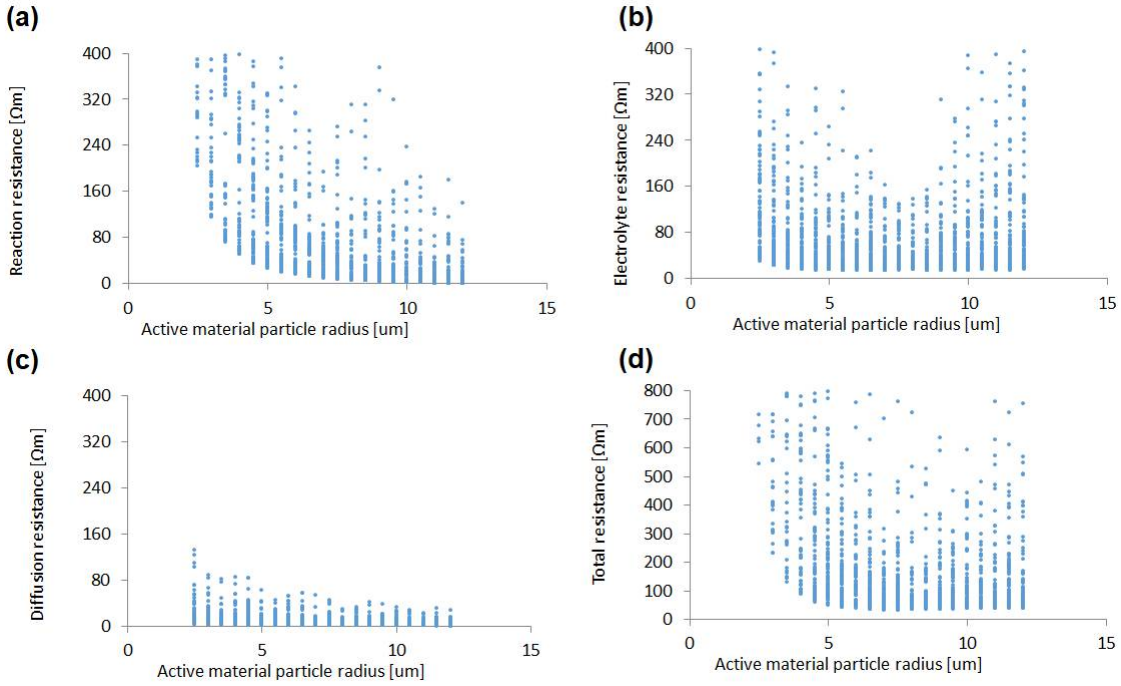

Figure 4. Sensitivities of (a) reaction resistance, (b) electrolyte resistance, (c) Li diffusion resistance, and (d) total resistance to the radius of the active material with total 2,100 simulation results.

Fig.5 shows the sensitivity of each resistance to the pressure in compaction process. The reaction resistance decreases exponentially as the pressure increases. This results from the fact that in the condition of higher pressure (larger overlap width) the volume fraction of the active material raises, thus the total surface area also increases. On the other hands, the electrolyte resistance increases in the system with higher volume fraction of the active material (lower volume fraction of pore). The diffusion resistance is relatively small to other resistances in each particle size in this study.

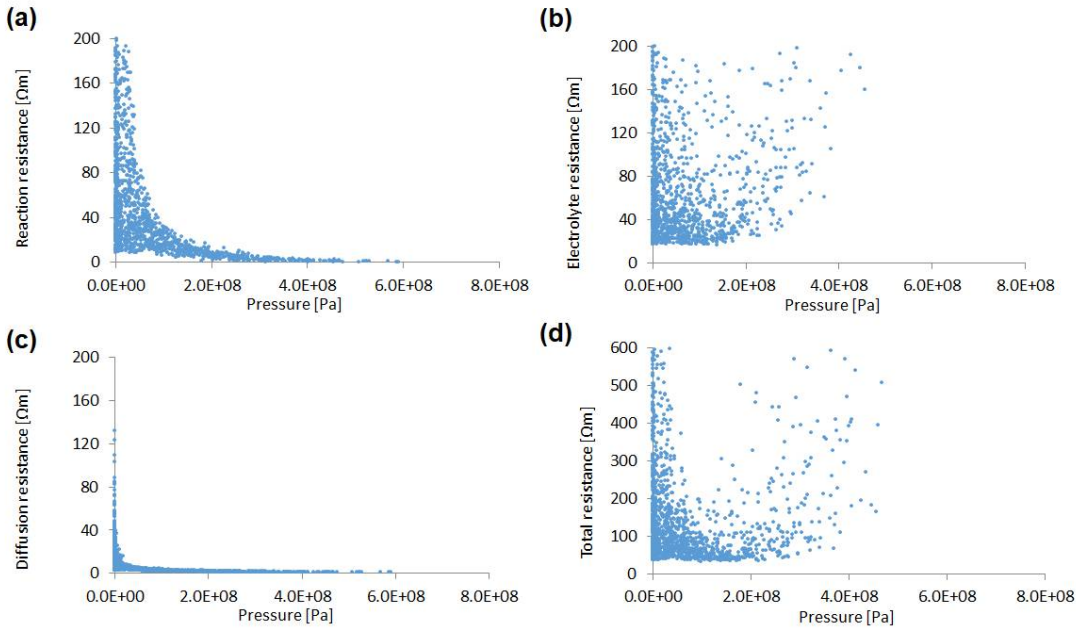

Figure 5. Sensitivities of (a) reaction resistance, (b) electrolyte resistance, (c) Li diffusion resistance, and (d) total resistance to the pressure with total 2,100 simulation results.

Preprints (www.preprints.org) | NOT PEER-REVIEWED | Posted: 1 April 2019 doi:10.20944/preprints201904.0016.v1

Peer-reviewed version available at Batteries 2019, 5, 54; doi:10.3390/batteries5030054

The binder/additives volume sensitivity of each resistance is illustrated in Fig.6. The reaction resistance increases linearly since the total surface area decreases with the ratio. Sigillary, approximately linear dependency of the binder/additives volume ratio is observed in the electrolyte resistance and the total resistance.

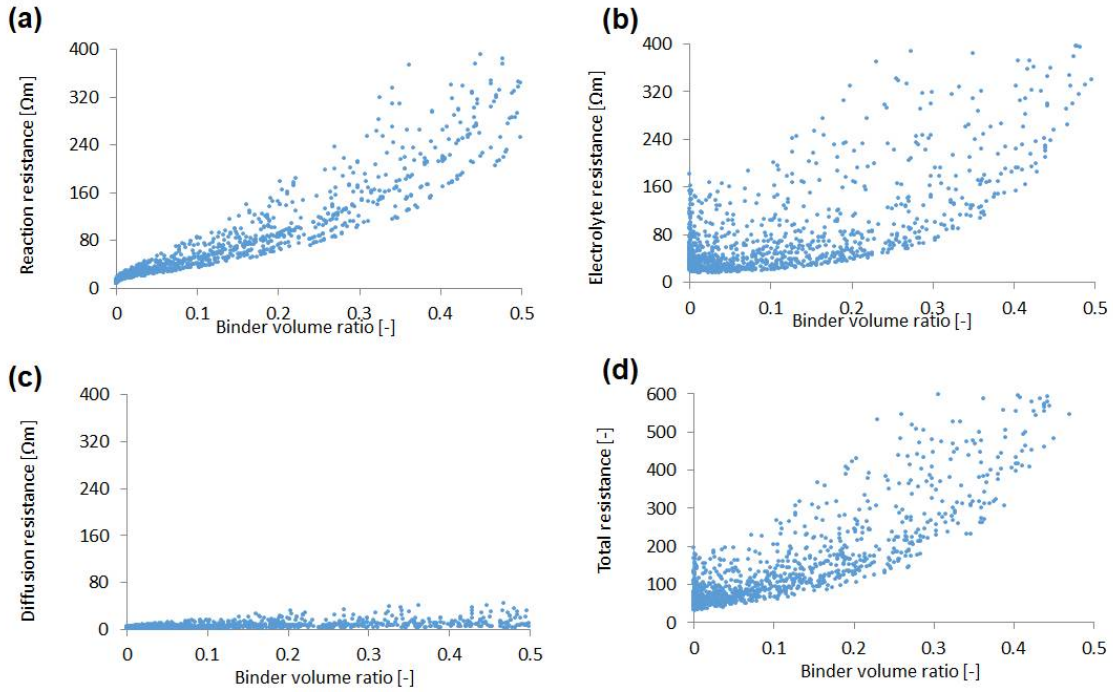

Figure 6. Sensitivities of (a) reaction resistance, (b) electrolyte resistance, (c) Li diffusion resistance, and (d) total resistance to the binder/additives volume ratio with total 2,100 simulation results.

3.2. Neural Network Regression

Various ANNs with different hyperparameters including number of neurons and hidden layers have been compared in order to determine the network configuration. The correlation coefficients R^2 for the validation data are listed in Table 3. R^2 values of ANNs which consists of two hidden layers is higher than the ones which consist of single layer, and saturates around 16 neurons.

Table 3. The correlation coefficients R^2 for the validation data.

Number of hidden layers	Number of neurons							
	2	4	6	8	10	12	16	20
1	0.326	0.788	0.834	0.810	0.790	0.978	0.937	0.979
2	0.330	0.795	0.822	0.863	0.827	0.845	0.990	0.990

Fig.7 shows the scatter plots of both training and test data between the resistances calculated by the simplified Physico-chemical models and the values predicted by various ANN models. As can be seen in this figures, the accuracy of prediction improves with the number of neurons and hidden layers. Although the ANN model which consists two hidden layers with 16 neurons (indicated as 16,16) predicts the both training and test data of the resistances accurately, the model was not suitable for the inverse problem by Bayesian optimization due to its instability. Therefore, we adopted the ANN model of (10, 10) for both the forward and inverse problem in this study.

Preprints (www.preprints.org) | NOT PEER-REVIEWED | Posted: 1 April 2019 doi:10.20944/preprints201904.0016.v1

Peer-reviewed version available at Batteries 2019, 5, 54; doi:10.3390/batteries5030054

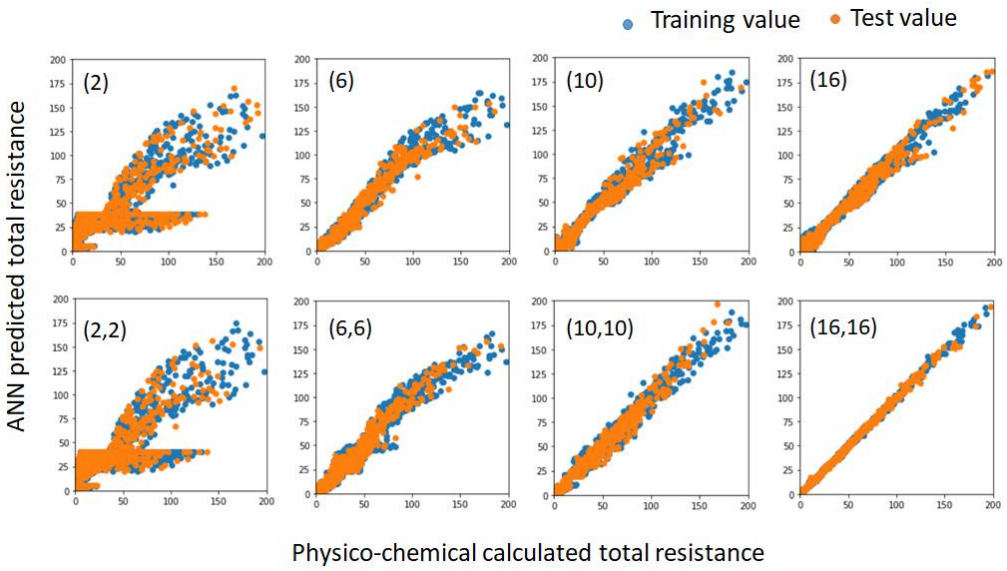

Figure 7. Scatter plots between the resistances calculated by the simplified Physico-chemical models and predicted by various ANN models with training data and test data.

It is useful to evaluate the effect of each design parameter, which includes volume ratio of the active material particles, radius of the active material particles, pressure in the compaction process and volume ratio binder/additives, on the total resistance as a guiding principle for manufacturing battery electrode. One of the simplest approaches for this purpose is to evaluate the weight coefficients of neurons on the first hidden layer of the ANN [27]. Here, we evaluate the summation of the weight coefficient magnitude $|w|$ of the first layer neurons for each input process parameter, shown in Fig.8. The graph shows that volume ratio of the active material particles has the largest impact on the total resistance although the effects of pressure and particle radius are relatively small. Note that these impact evaluations assume the physical parameters listed in Table.1. In other words, these values may change in other conditions.

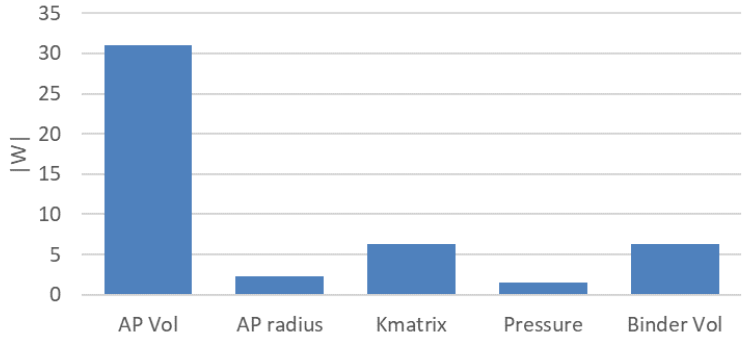

Figure 8. Comparison of summations of the weight coefficient magnitudes on the first layer neurons for various design parameter.

3.3. Process parameters optimized by Bayesian optimization

Optimized process parameters have been inferred from the total resistance using Bayesian optimization with the constructed ANN model. In order to confirm validation of optimization, five calculations have been performed with different initial conditions. Fig. 9 indicates the convergence plot of each initial condition with optimization. Each calculation almost come to converge within 100 iterations to around 47 [Ωm^2].

Preprints (www.preprints.org) | NOT PEER-REVIEWED | Posted: 1 April 2019 doi:10.20944/preprints201904.0016.v1

Peer-reviewed version available at Batteries 2019, 5, 54; doi:10.3390/batteries5030054

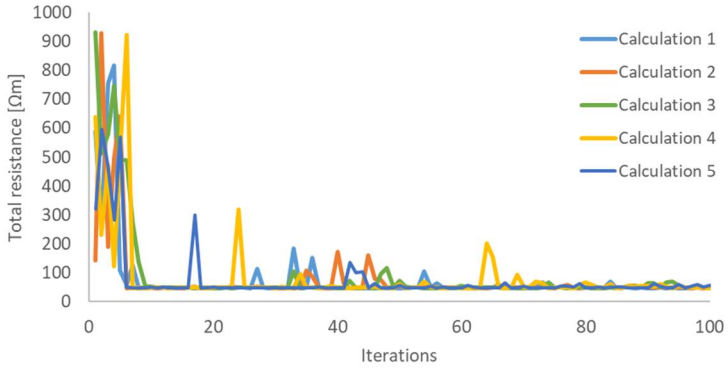

Figure 9. Convergence plot of five different initial conditions within 100 iterations.

The optimized process parameters for the total resistance is shown in Table 4. The results suggest that the active material composed of small size particles should be packed near 50% with small amount of binder/additives. The highest ionic conductivity in range of this study is suggested since the higher ionic conductivity of electrolyte is, the more total resistance of the electrode decreases. The proposed compaction pressure 459 [MPa] is within the typical range in actual process [28]. Note, however, that negative effect of applying pressure is not taken into account in this model, such as damage of foil and active materials.

Fig. 10 (a) shows the packing structure of the active material particles in the condition of the optimized process parameters. Radar chart of each normalized resistance in various process parameters is shown in Fig. 10 (b). The red triangle indicates the optimized (the smallest total resistance) parameter set and other colors indicate other combinations. Note that the reaction resistance in the optimized parameters is smaller than the values in other parameters although the diffusion and the electrolyte resistance are not the smallest in the optimized process parameters.

It should be emphasized that these optimized parameters strongly depend on assumed physical parameters including diffusion coefficient in active material, exchange current density *etc.* Nevertheless, we believe that the proposed scheme for prediction of electrode resistance and optimization is also useful in various physical parameters.

Table 4. Optimized process parameters for the total resistance.

Active material		Binder/ additives	Electrolyte	Compaction
Volume fraction [%]	Radius [um]	Volume ratio [%]	Conductivity [S/m]	Pressure [MPa]
50.4	6.00	0.0820	1.00	590

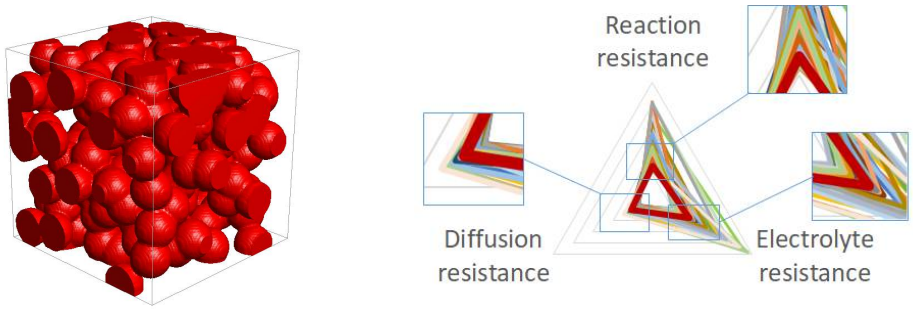

Figure 10. (a) Packing structure of the active material particles and (b) radar chart of each resistance factor in the condition of the optimized process parameters.

Preprints (www.preprints.org) | NOT PEER-REVIEWED | Posted: 1 April 2019 doi:10.20944/preprints201904.0016.v1

Peer-reviewed version available at Batteries 2019, 5, 54; doi:10.3390/batteries5030054

3.4. Optimized process parameters in higher capacity

In order to predict the optimized process parameters for higher capacity electrode, we have conducted further calculations using the ANN model and optimization scheme described in section 3.3. The discharge resistances have been predicted in the condition that the active material volume fraction are fixed from 0.5 to 0.8. Fig.11 shows the dependence of (a) Resistance, (b) Pressure in compaction process, (c) Active material radius and (d) Binder/additives on the volume ratio of the active material, respectively. One can see that the total resistance increases exponentially with the volume ratio of the active material (see Fig.11 (a)). On the other hand, the process parameters are almost unchanged from the values of active material volume fraction 0.5 although the active material particle radius and the binder/additives volume ratio slightly fluctuate. This result indicates that the optimized process parameters in the global condition (the volume ratio of the active material is not fixed, listed in Table.4) are the best values also in the higher capacity conditions.

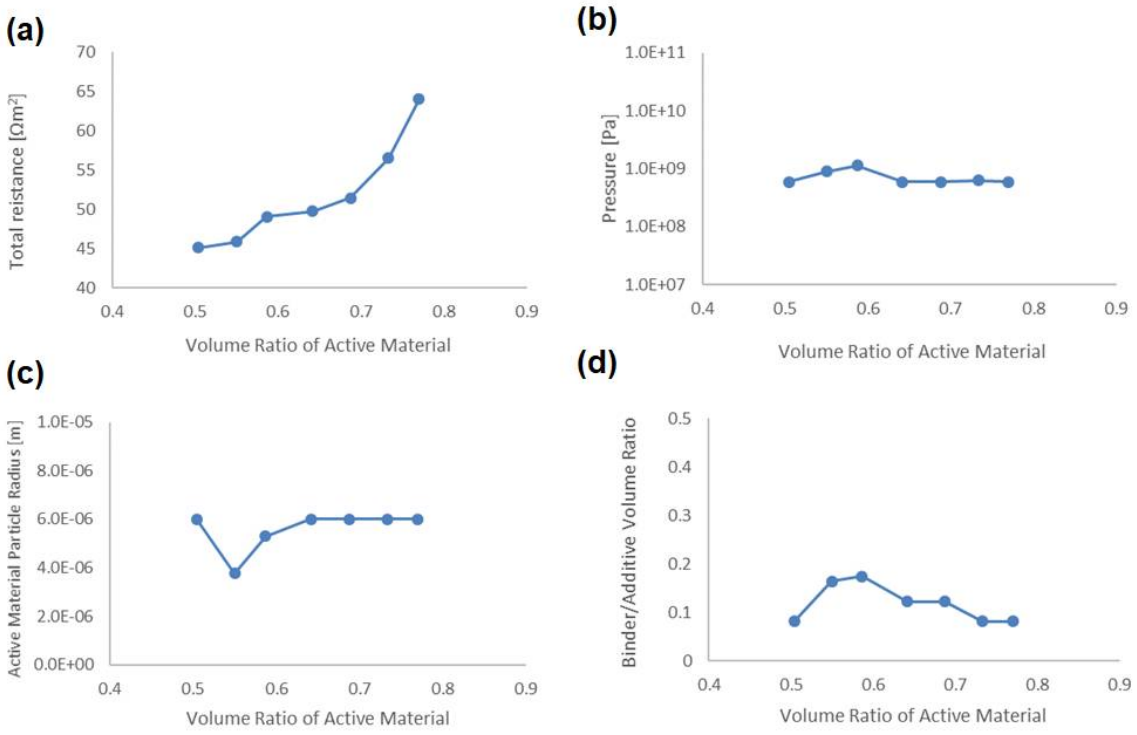

Figure 11. Dependences to the volume ratio of the active material of (a) Total resistance, (b) Pressure in compaction process, (c) Active material radius and (d) Binder/additives.

5. Conclusions

In this study, the prediction and optimization scheme of battery porous electrode has been proposed as a guiding principle for manufacturing process. First, High-throughput simulation model based on simplified Physico-chemical equations with artificial 3D structures composed of random packed spheres has been constructed and over 2000 calculations were conducted. The sensitivity analyses for the calculation results indicate that the total resistance, which is summation of the reaction, electrolyte and diffusion results, has minimum value to the volume ratio of the active material particles, their radius and pressure in compact process, respectively.

Next, the regression models via Artificial Neural Network have been created in order to predict charge/discharge resistance by various process parameters including the active material volume ratio, their particle radius, pressure in compact process and binder/additives volume ratio, using simulation results of these artificial 3D structures. The accuracy of prediction improves with the number of neurons and hidden layers, and the ANN model which consists two hidden layers with 16 neurons predict the both training and test data of the resistances accurately.

Finally, optimized process parameters have been inferred from the total resistance using Bayesian optimization with the ANN model. The results indicated that the active material composed of small size particles should be packed near 50% with small amount of binder/additives. As results of further calculations in the conditions that the active material volume fraction is fixed from 0.5 to 0.8, this parameter set is the best also in the higher capacity conditions.

Although the optimized parameters strongly depend on assumed physical parameters including diffusion coefficient in active material, exchange current density *etc.* Nevertheless, the proposed scheme for prediction of electrode resistance and optimization is also useful in various physical parameters and conditions.

References

1. Etacheri,V.; Marom,R.; Elazari, R.; Salitra, G.; Aurbach, D. Challenges in the development of advanced Li-ion batteries: a review. *Energy & Environmental Science* **2011**, 4 (9), pp. 3243-3262.
2. Lu, L.; Han, X.; Li, J.; Hua, J.; Ouyang, M. *Journal of Power Sources* **2013**, 226, 15, pp. 272-288.
3. Long, W. J; Dunn, B.; Rolison, R. D.; White, S. H. Three-Dimensional Battery Architectures, *Chemical Reviews* **2004**, 104, No. 10, pp. 4463-4492.
4. Arthur, S. T.; Bates, J. D.; Cirigliano, N.; Johnson, C. D.; Malati, P.; Mosby, M. J.; Perre, E.; Rawls, T. M.; Prieto, L. A.; Dunn, B. Three-dimensional electrodes and battery architectures. *MRS BULLETIN* **2011**, 36, pp. 523-531.
5. Doyle, M.; Newman, J. Comparison of modeling predictions with experimental data from plastic Lithium Ion cells. *Journal of Electrochemical Society* **1996**, 143, No.6, pp. 1890-1903.
6. Fang, W.; Kwon, J. O.; Wang, Y. C. Electrochemical–thermal modeling of automotive Li-ion batteries and experimental validation using a three-electrode cell. *International Journal of Energy Research* **2010**, 34, pp. 107-115.
7. Ning, G.; Popov N. B. Cycle Life Modeling of Lithium-Ion Batteries. *Journal of the Electrochemical Society* **2004**, 151 (10) pp. A1584-A1591.
8. Ramadass, P.; Haran, B.; Gomadam, M. P.; White, R.; Popov, N. B. Development of First Principles Capacity Fade Model for Li-Ion Cells. *Journal of the Electrochemical Society* **2004**, 151 (2), pp. A196-A203.
9. Takagishi, Y.; Yamaue, T. Predicgtion of Li-ion Battery Module Performance under Running Condition Based on "Multifactorial Degradation Model". *International Journal of Automotive Engineering* **2017**, 8, 3, pp. 137-142.
10. Melcher, A.; Ziebert, C.; Magnus, R.; Seifert, J. H. Modeling and Simulation of the Thermal Runaway Behavior of Cylindrical Li-Ion Cells—Computing of Critical Parameters. Energies **2016**, 9, 292.
11. Abada, S.; Marlair, G.; Lecocq, A.; Petit, M.; Sauvant-Moynot, V.; Safety focused modeling of lithium-ion batteries: A review. *Journal of Power Sources* **2016**, 306, pp.178-192.
12. Less, G. B.; Seo, H. J.; Han, S.; Sastry, M. A.; Zausch, J.; Latz, A.; Schmidt, S.; Wieser, C.; Kehrwald, D.; Fell, S.; Micro-Scale Modeling of Li-ion Batteries: Parameterization and Validation. *Journal of The Electrochemical Society* **2012**, 159 (6) pp. A697-A704.
13. Gelb, J.; Finegan, P. D.; Brett, L. J. D.; Shearing, R. P. Multi-scale 3D investigations of a commercial 18650 Li-ion battery with correlative electron- and X-ray microscopy. *Journal of Power Sources* 2017, 357, 31, pp. 77-86.
14. Trembacki, L. B.; Mistry, N. A.; Noble, R. D.; Ferraro, E. M.; Mukherjee, P. P.; Roberts, A. S. Mesoscale Analysis of Conductive Binder Domain Morphology in Lithium-Ion Battery Electrodes. *Journal of The Electrochemical Society* **2018**, 165 (13) pp. E725-E736.

15. Danner, T.; Singhc, M.; Hein S.; Kaiserc, J.; Hahn, H.; Latz, A. Thick electrodes for Li-ion batteries: A model based analysis. *Journal of Power Sources* **2016**, 334, 1, pp. 191-201.
16. Hosseinzadeh, E.; Marco, J.; Jennings, P. Electrochemical-Thermal Modelling and Optimization of Lithium-Ion Battery Design Parameters Using Analysis of Variance. Energies **2017**, 10, 1278.
17. Dawson-Elli, N.; Lee,S. B.; Pathak, M.; Mitra, K.; Subramanian R. V. Data Science Approaches for Electrochemical Engineers: An Introduction through Surrogate Model Development for Lithium-Ion Batteries. *Journal of The Electrochemical Society* **2018**, 165 (2) pp. A1-A15.
18. Bertei, A.; Nucci, B.; Nicolella, C. Effective Transport Properties in Random Packings of Spheres and Agglomerates. *CHEMICAL ENGINEERING TRANSACTIONS* **2013**, 32, pp. 1531-1536.
19. Persson, J. N. B. Contact mechanics for randomly rough surfaces. *Surface Science Reports* **2006**, 61, pp. 201–227
20. Schneider, M.; Hofmann, T.; Andrä, H.; Lechner, P.; Ettemeyer, F.; Volk, W.; Steeb, H. Modelling the microstructure and computing effective elastic properties of sand core materials. *International Journal of Solids and Structures* **2018**, 143, pp. 1-17.
21. GeoDict, Math2Market GmbH, Kaiserslautern, Germany. Accessed: -09-01 http:// www.geodict.de . 2017.
22. Tibshirani, R.; Regression shrinkage and selection via the lasso. *Journal of the Royal Statistical Society: Series B (Statistical Methodology)* **1996**, vol. 58, no. 1, pp. 267-288.
23. Hoerl, E. A.; Kennard, W. R.; Ridge Regression: Biased Estimation for Nonorthogonal Problems. *Technometrics*. **1970**, 12, No. 1, pp. 55-67.
24. Donato, R. H. T.; Quiles, G. M. Machine learning systems based on xgBoost and MLP neural network applied in satellite lithium-ion battery sets impedance estimation. *Advanced Computational Intelligence: An International Journal*. 5, No.1, pp. 1-20.
25. Pedregosa, F.; Varoquaux, G.; Gramfort, A.; Michel, V.; Thirion, B; Grisel, O.; Blondel, M.; Prettenhofer, P.; Weiss, R.; Dubourg, V.; Vanderplas, J.; Passos, A.; Cournapeau, D.; Brucher, M.; Perrot, M.; Duchesnay, E.; Scikit-learn: Machine Learning in Python. *JMLR* **2011**, 12, pp. 2825-2830.
26. Hensman, J.; Fusi, N.; Andrade, R.; Durrande, N.; Saul, A.; Lawrence, N.D. (2012). GPy. github.com/SheffieldML/GPy.
27. Wu, B.; Han, S.; G. K. Shin.; Lu, W. Application of aritificial neural network in design of lithium-ion batteries. *Journal of The Electrochemical Society* **2018**, 395, pp. 128-136.
28. Trana, Y. H.; Grecoa, G.; Täubert, C.; Wohlfahrt-Mehrens, M.; Haselrieder, W.; Kwade, A. Influence of electrode preparation on the electrochemical performance of $LiNi_{0.8}Co_{0.15}Al_{0.05}O_2$ composite electrodes for lithium-ion batteries. *Journal of Power Sources* **2012**, 210, pp. 276–285.